UC Berkeley
UC Berkeley Previously Published Works

Title
A Compact Model of Antiferroelectric Capacitor

Permalink
https://escholarship.org/uc/item/8p63d5bg

Journal
IEEE Electron Device Letters, 43(2)

ISSN
0741-3106

Authors
Tung, Chien-Ting
Salahuddin, Sayeef
Hu, Chenming

Publication Date
2022-02-01

DOI
10.1109/led.2021.3135001

Copyright Information
This work is made available under the terms of a Creative Commons Attribution-NonCommercial-NoDerivatives License, available at
https://creativecommons.org/licenses/by-nc-nd/4.0/

Peer reviewed

eScholarship.org Powered by the California Digital Library
University of California

A Compact Model of Antiferroelectric Capacitor

Chien-Ting Tung, *Graduate Student Member, IEEE*, Sayeef Salahuddin, *Fellow, IEEE,* and Chenming Hu, *Life Fellow, IEEE*

***Abstract*— In this paper, we develop a compact model of antiferroelectric (AFE) capacitors. AFE material, similar to the ferroelectric (FE) material, is a good candidate for non-volatile memory applications. Unlike FE materials, there are no good compact models that can describe the AFE materials for circuit simulation. In this study, we consider the AFE material as a collection of multiple crystal groups. For each group, the polarization may switch from zero to positive or negative polarization and vice versa depending on the electric field polarity. This switching is modeled by a local field-dependent switching rate, which has a statistical distribution among the groups. We implement this model in Verilog-A and run it on a commercial SPICE simulator to demonstrate this model's capability to reproduce the published experimental data of the dependency of the AFE capacitor switching on the writing pulse width and voltage and the major and minor loops behavior are demonstrated.**

***Index Terms*— Compact model, antiferroelectric, hafnium zirconium oxide (HZO)**

I. INTRODUCTION

Antiferroelectric (AFE) material is a promising material for memory applications in integrated circuit (IC) industry. Compared to FE material, experiments have shown that zirconium oxide (ZrO_2) based AFE has higher speed and endurance compared to FE [1, 2]. Furthermore, the double hysteresis loops of AFE may potentially store two bits of data per device, doubling the storage density [3]. AFE can be applied to the nonvolatile memories (NVMs) such as ferroelectric RAM (FERAM), ferroelectric tunnel junction (FTJ) and ferroelectric FET (FEFET) with better reliability [4]. AFE also shows great potential for energy storage supercapacitor applications [5]. AFE-DRAM has been demonstrated to have 10ns switching-speed and 1ms-retention, and high endurance with 10^{12} cycles [6]. Moreover, AFE can be stacked with FE to engineer the on-current and subthreshold swing of negative capacitance FET (NCFET) [7, 8].

This work was supported by the Berkeley Device Modeling Center, University of California at Berkeley, Berkeley, CA, USA. The review of this article was arranged by Editor XXX. (Corresponding author: Chien-Ting Tung.)

The authors are with the Department of Electrical Engineering and Computer Sciences, University of California at Berkeley, Berkeley, CA 94720 USA (e-mail: cttung@berkeley.edu).

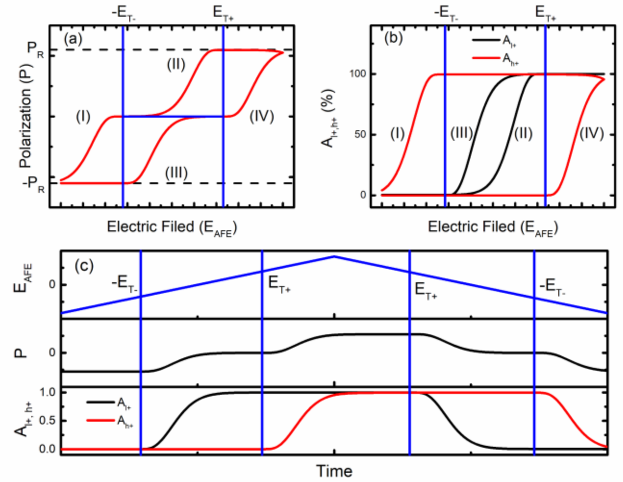

Fig. 1. (a) The schematic hysteresis loop of AFE which is divided into 4 regions: (I) $E_{\text{AFE}} < -E_{\text{T}-}$, (II) $-E_{\text{T}-} \le E_{\text{AFE}} \le E_{\text{T}+}$ & $P > 0$, (III) $-E_{\text{T}-} \le E_{\text{AFE}} \le E_{\text{T}+}$ & $P < 0$, and (IV) $E_{\text{AFE}} > E_{\text{T}+}$; (b) The percentage of $A_{\text{l}+}$ and $A_{\text{h}+}$ over A_{l} and A_{h} under different E_{AFE} ; (c) The schematic transient diagram of AFE.

To model AFE, the best-known model is the Kittel's model [9]. However, similar to the Landau–Khalatnikov (L–K) equation [10-12], to simulate the multi-domain dynamics using phase-field modeling is orders of magnitude too time-consuming for IC simulation. Moreover, in HZO thin film, the polycrystalline property makes the device contain multiple grains with different material properties due to the crystal orientation, stoichiometry and stress [2, 13]. Thus, not only the multi-domain but also multi-grain physics needs to be considered. Another common model is Preisach model [14, 15]. It uses empirical interpolation to produce the hysteresis loop, which is not physical. Therefore, we aim to develop a computationally efficient model that considers the multi-domain/multi-grain switching physics in AFE.

Multi-grain switching has been studied in FE for many years, and one model is the nucleation-limited-switching (NLS) model [16-18]. It considers a FE capacitor made of many independent grains and each grain has a unique exponentially time-dependent switching rate. The NLS model has also been used on AFE [2, 19] but these models can only characterize (positive or negative) half of the major hysteresis loop and not any minor loops. In this paper, based on our previous model of FE capacitor [20], we construct an AFE model that reimagines NLS switching dynamics for AFE. We show that this model can model both major loop and minor loop as well as the pulse-width-dependent switching characteristics well by reproducing the published experimental data [1, 14].

II. Model

In AFE, we can observe from Fig. 1 that the polarization has three different states: P_R , $-P_R$ and 0. Polarization would switch from $-P_R$ to 0 and from 0 to P_R while voltage increases and vice versa. For each hysteresis loop, we can refer to FE domain switching that the polarization switches from nuclei and grow to the entire device [11, 12]. For example, for the left hysteresis curve in Fig. 1a, the negative polarization would switch into zero polarization from some nuclei and switch the whole area when voltage increases, *which the capacitor is switched from negatively polarized areas into non-polarized areas*. Therefore, we approximate the total polarization into the combination of positively polarized areas A_+ , negatively polarized areas A_- and non-polarized areas A_0 . We first derive the switching current in region (I) in Fig. 1 as (1a) where E_{AFE} is the electric field, E_{T+} and E_{T-} are the threshold electric field, and P_R is the remanent polarization. However, directly solving three kinds of areas is numerically complex and not acceptable for a compact model. Instead, we introduce two new areas by dividing the capacitor into low-field-switching area A_l and high-field-switching area A_h where A_l starts switching under the low voltage in (II) & (III), and A_h starts switching under the higher voltage in region (I) & (IV), and $A_l = A_h = 0.5A_T$ where A_T is the total area. A_l and A_h only consist of positively and negatively polarized areas, A_{l+}, A_{l-}, A_{h+}, and A_{h-} . A_0 can be represented by the polarization cancellation between A_h and A_l . Fig. 1 shows how A_{l+} and A_{h+} varying with E_{AFE} in which we can see how polarization changes corresponding to A_h and A_l . Then, we obtain the switching current in (I) as (1a). Similarly, the switching current in region (IV) is shown in (1b). For regions (II) & (III), the derivation is simpler. Depending on the polarization P , we either calculate the decrease in A_{l+} or A_{l-} as (1c).

$$I(A_0 \to A_-) + I(A_+ \to A_0) \cong I(A_{l+} \to A_{l-}) + I(A_{h+} \to A_{h-}) = 2P_R\left[\frac{dA_{l+}}{dt} + \frac{dA_{h+}}{dt}\right], \tag{1a}$$

$$I(A_0 \to A_+) + I(A_- \to A_0) \cong -2P_R\left[\frac{dA_{l-}}{dt} + \frac{dA_{h-}}{dt}\right], \tag{1b}$$

$$\begin{aligned} I(A_+ \to A_0) &= 2P_R\frac{dA_{l+}}{dt}, \text{ if } P > 0 \\ I(A_- \to A_0) &= -2P_R\frac{dA_{l-}}{dt}, \text{ if } P < 0 \end{aligned} \tag{1c}$$

After deriving the current expressions, we now set up the differential equations for each grain group. A_η is the total area of which the switching rate is characterized by the random variable η shown in (3). η has a mean of 1 and a statistical distribution $f(\eta)$ to be determined from measurement data [20].

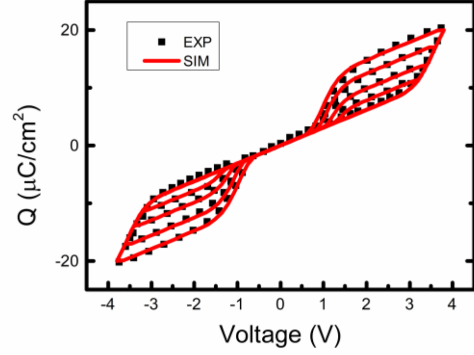

Fig. 2. Modeled hysteresis curve of a 10 nm ZrO_2 capacitor from [14] with $P_R = 11\mu C/cm^2$, $\tau_0 = 100ps$, $E_a = 3.45MV/cm$, $E_{T+} = E_{T-} = 2.26MV/cm$ and $\alpha = 2.46$.

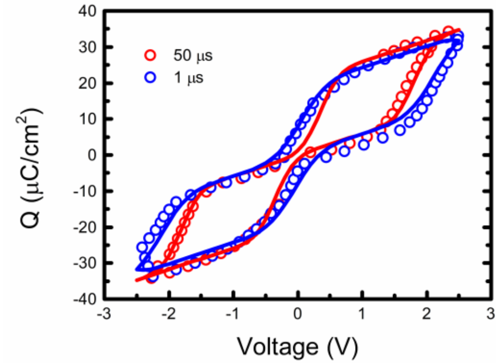

Fig. 3. Modeled hysteresis curve of a 6 nm HZO capacitor from [1] with $P_R = 20\mu C/cm^2$, $\tau_0 = 1.5ns$, $E_a = 3.6MV/cm$, $E_{T+} = E_{T-} = 1.8MV/cm$ and $\alpha = 1.7$.

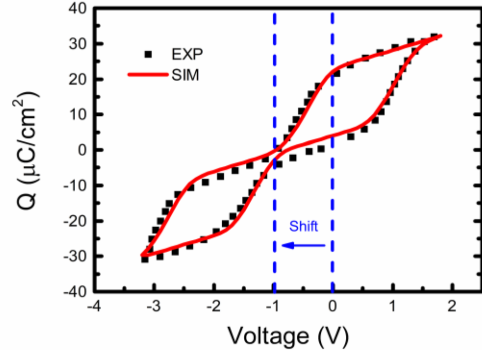

Fig. 4. Modeled hysteresis curve of a $TiN/TiO_2/HZO/RuO_2/HfO_2$ -stacked capacitor from [1] with $P_R = 20\mu C/cm^2$, $\tau_0 = 2ns$, $E_a = 3.7MV/cm$, $E_{T+} = 1.9MV/cm$, $E_{T-} = 2.3MV/cm$ and $\alpha = 1.7$.

Here, we assume a Gaussian distribution. Since $A_{\eta+} = A_\eta - A_{\eta-}$, we can write all differential equations in terms of $A_{\eta+}$ as (2). The switching time constant is defined in (3) known as the Merz's law [21] where τ_0 is the characteristic time at a very large field, E_a is the mean activation field, α is a fitting parameter, and $E_{eff,l}$ is the effective electric field which equals $E_{AFE} - E_{T+}$ at (III) & (IV) and $E_{AFE} + E_{T-}$ at (I) & (II), and $E_{eff,h}$ equals to $E_{AFE} - E_{T+}$ at (IV) and $E_{AFE} + E_{T-}$ at (I)

where E_{T+} and E_{T-} are fitting parameters that characterize the difference between the fast-switching and slow-switch areas. We keep tracking $A_{\eta l+}$ and $A_{\eta h+}$ with time using the differential equations (2). Finally, the overall positively polarized area A_{+} is the summation of all $A_{\eta +}$ where the integration is carried out numerically using (4). The polarization and current are calculated by (5) and (6) respectively where C_{AFE} is the background capacitance of the AFE capacitor.

$$\begin{aligned} \frac{dA_{\eta +}}{dt} &= \frac{d\left(A_{\eta l+}+A_{\eta h+}\right)}{dt} = \frac{-A_{\eta l+}}{\tau_l} + \frac{-A_{\eta h+}}{\tau_h}, \text{ if } E_{AFE} \le -E_{T-} \\ &= \frac{-A_{\eta l+}}{\tau_l}, \text{ if } -E_{T-} < E_{AFE} < E_{T+} \ \& \ P > 0 \\ &= \frac{A_{\eta l} - A_{\eta l+}}{\tau_l}, \text{ if } -E_{T-} < E_{AFE} < E_{T+} \ \& \ P < 0 \\ &= \frac{A_{\eta l} - A_{\eta l+}}{\tau_l} + \frac{A_{\eta h} - A_{\eta h+}}{\tau_h}, \text{ if } E_{AFE} \ge E_{T+}, \end{aligned} \tag{2}$$

$$\tau_l = \tau_0 \exp\left[\left(\frac{\eta E_a}{\left|E_{eff,l}\right|}\right)^{\alpha}\right], \ \tau_h = \tau_0 \exp\left[\left(\frac{\eta E_a}{\left|E_{eff,h}\right|}\right)^{\alpha}\right], \tag{3}$$

$$A_{+}(t) = \sum A_{\eta +}(t) \cong \int_0^{\eta \max} A_T f(\eta)\, d\eta \times \frac{A_{\eta +}(t)}{A_\eta}, \tag{4}$$

$$P(t) = P_R \times \left(\frac{2A_{+}(t)}{A_T} - 1\right), \tag{5}$$

$$I(t) = 2P_R \frac{dA_{+}(t)}{dt} + C_{AFE}\frac{dV_{AFE}}{dt}, \tag{6}$$

III. Results

We implement this model with Verilog-A and run simulations on Hspice. To verify this compact model's accuracy, we fit the data of a 10 nm ZrO_2 capacitor subject to a triangle voltage waveform at 1 kHz with varying amplitude [14]. In parameter extraction, we first extract P_R, E_{T+} and E_{T-} which can be easily found as Fig. 1. For other parameters, τ_0 can be extracted at the high applied voltage; E_a and α can be extracted by tuning the fitting of switching polarization under different voltages. The more detailed fitting process can be analogous to the FE model [16, 18]. In Fig. 2, our model results are in excellent agreement with the experimental data. It successfully captures the minor loop switching of AFE by tracking the polarization history. Furthermore, we test the model with different rise/fall time. Fig. 3 shows the measurement and fitting of a 6 nm HZO with a rise/fall time of 50 μs and 1 μs [1]. When the ramp rate is fast enough, A_{l+} will not completely switch to A_{l-} and compensate A_{h+}, which let us can model the polarization retention at high speed. These demonstrations show that this model can reproduce the switching dynamics under various measurement conditions. In addition, we model the TiN/TiO_2/HZO/RuO_2/HfO_2 -stacked AFE [1] with 5 nm HZO and 0.5 nm TiO_2 in Fig. 4. The RuO_2 layer's high work function shifts the nonvolatile states from 0 V to -1V. To simulate this device, we also use the model's capability of accepting a series capacitance (TiO_2) and the work function difference. Fig. 4 shows the fitting result.

IV. Conclusion

We present a compact model of AFE capacitors. This model produces the AFE behaviors with the switching dynamics between positive- polarized, negative-polarized and non-polarized states in each grain group in an AFE capacitor. This model computes the time-dependent polarization switching history through the entire simulated time period of the capacitor operation. We demonstrate the model's capability to capture the major and minor loop switching as well as the speed-dependent hysteresis loop of AFE capacitors. We also show that this model can simulate the nonvolatile AFE stack, which is interested in future NVM applications.

References

[1] Y. Goh, J. Hwang, and S. Jeon, "Excellent Reliability and High-Speed Antiferroelectric HfZrO2 Tunnel Junction by a High-Pressure Annealing Process and Built-In Bias Engineering," *ACS Appl Mater Interfaces,* vol. 12, no. 51, pp. 57539-57546, Dec 23, 2020.

[2] M. Si, X. Lyu, P. R. Shrestha, X. Sun, H. Wang, K. P. Cheung, and P. D. Ye, "Ultrafast measurements of polarization switching dynamics on ferroelectric and anti-ferroelectric hafnium zirconium oxide," *Applied Physics Letters,* vol. 115, no. 7, 2019.

[3] M. M. Vopson, and X. Tan, "Four-State Anti-Ferroelectric Random Access Memory," *IEEE Electron Device Letters,* vol. 37, no. 12, pp. 1551-1554, 2016.

[4] M. Pesic, U. Schroeder, S. Slesazeck, and T. Mikolajick, "Comparative Study of Reliability of Ferroelectric and Anti-Ferroelectric Memories," *IEEE Transactions on Device and Materials Reliability,* vol. 18, no. 2, pp. 154-162, 2018.

[5] S.-H. Yi, H.-C. Lin, and M.-J. Chen, "Ultra-high energy storage density and scale-up of antiferroelectric TiO2/ZrO2/TiO2 stacks for supercapacitors," *Journal of Materials Chemistry A,* vol. 9, no. 14, pp. 9081-9091, 2021.

[6] S.-C. Chang, N. Haratipour, S. Shivaraman, T. L. Brown-Heft, J. Peck, C.-C. Lin, I. C. Tung, D. R. Merrill, H. Liu, C.-Y. Lin, F. Hamzaoglu, M. V. Metz, I. A. Young, J. Kavalieros, and U. E. Avci, "Anti-ferroelectric HfxZr1-xO2 Capacitors for High-density 3-D Embedded-DRAM," in 2020 IEEE International Electron Devices Meeting (IEDM), 2020, pp. 28.1.1-28.1.4.

[7] S.-E. Huang, P. Su, and C. Hu, "S-Curve Engineering for ON-State Performance Using Anti-Ferroelectric/Ferroelectric Stack Negative-Capacitance FinFET," *IEEE Transactions on Electron Devices,* vol. 68, no. 9, pp. 4787-4792, 2021.

[8] M. H. Lee, K.-T. Chen, C.-Y. Liao, G.-Y. Siang, C. Lo, H.-Y. Chen, Y.-J. Tseng, C.-Y. Chueh, C. Chang, Y.-Y. Lin, Y.-J. Yang, F.-C. Hsieh, S. T. Chang, M.-H. Liao, K.-S. Li, and C. W. Liu, "Bi-directional Sub-60mV/dec, Hysteresis-Free, Reducing Onset Voltage and High Speed Response of Ferroelectric-AntiFerroelectric Hf0.25Zr0.75O2 Negative Capacitance FETs," in 2019 IEEE International Electron Devices Meeting (IEDM), San Francisco, CA, USA, 2019, pp. 23.6.1-23.6.4.

[9] C. Kittel, "Theory of Antiferroelectric Crystals," *Physical Review,* vol. 82, no. 5, pp. 729-732, 1951.

[10] L. D. Landau, and I. M. Khalatnikov, "On the anomalous absorption of sound near a second order phase transition point," *Dokl. Akad. NaukSSSR,* vol. 96, pp. 469-472, May, 1954.

[11] S. Smith, K. Chatterjee, and S. Salahuddin, "Multidomain Phase-Field Modeling of Negative Capacitance Switching

Transients," *IEEE Transactions on Electron Devices,* vol. 65, no. 1, pp. 295-298, 2018.

[12] A. K. Saha, K. Ni, S. Dutta, S. Datta, and S. Gupta, "Phase field modeling of domain dynamics and polarization accumulation in ferroelectric HZO," *Applied Physics Letters,* vol. 114, no. 20, 2019.

[13] J. Muller, T. S. Boscke, U. Schroder, S. Mueller, D. Brauhaus, U. Bottger, L. Frey, and T. Mikolajick, "Ferroelectricity in Simple Binary ZrO2 and HfO2," *Nano Lett,* vol. 12, no. 8, pp. 4318-23, Aug 8, 2012.

[14] Z. Wang, J. Hur, N. Tasneem, W. Chern, S. Yu, and A. Khan, "Extraction of Preisach model parameters for fluorite-structure ferroelectrics and antiferroelectrics," *Sci Rep,* vol. 11, no. 1, pp. 12474, Jun 14, 2021.

[15] A. K. Saha, and S. K. Gupta, "Modeling and Comparative Analysis of Hysteretic Ferroelectric and Anti-ferroelectric FETs," in 2018 76th Device Research Conference (DRC), Santa Barbara, CA, USA, 2018, pp. 1-2.

[16] C. Alessandri, P. Pandey, A. Abusleme, and A. Seabaugh, "Monte Carlo Simulation of Switching Dynamics in Polycrystalline Ferroelectric Capacitors," *IEEE Transactions on Electron Devices,* vol. 66, no. 8, pp. 3527-3534, Aug., 2019.

[17] C. Alessandri, P. Pandey, A. Abusleme, and A. Seabaugh, "Switching Dynamics of Ferroelectric Zr-Doped HfO2," *IEEE Electron Device Letters,* vol. 39, no. 11, pp. 1780-1783, Nov., 2018.

[18] S. D. Hyun, H. W. Park, Y. J. Kim, M. H. Park, Y. H. Lee, H. J. Kim, Y. J. Kwon, T. Moon, K. D. Kim, Y. B. Lee, B. S. Kim, and C. S. Hwang, "Dispersion in Ferroelectric Switching Performance of Polycrystalline Hf0.5Zr0.5O2 Thin Films," *ACS Appl Mater Interfaces,* vol. 10, no. 41, pp. 35374-35384, Oct. 17, 2018.

[19] C. Liu, S. X. Lin, M. H. Qin, X. B. Lu, X. S. Gao, M. Zeng, Q. L. Li, and J. M. Liu, "Energy storage and polarization switching kinetics of (001)-oriented Pb0.97La0.02(Zr0.95Ti0.05)O3 antiferroelectric thick films," *Applied Physics Letters,* vol. 108, no. 11, 2016.

[20] C. T. Tung, G. Pahwa, S. Salahuddin, and C. Hu, "A Compact Model of Polycrystalline Ferroelectric Capacitor," *IEEE Transactions on Electron Devices*, pp. 1-4, 2021.

[21] W. J. Merz, "Domain Formation and Domain Wall Motions in Ferroelectric BaTiO3Single Crystals," *Physical Review,* vol. 95, no. 3, pp. 690-698, 1954.